Microstructured Fibers for Sensing

Nan Zhang, Georges Humbert, and Zhifang Wu

Abstract Microstructured optical fibers (MOFs), which have a holey structure in the cladding/core region, exhibit enhanced sensing sensitivity and performance for liquid/gas samples. In MOFs, the presence of sensing samples in the holey cladding/core region increases mode-field overlap and effective interaction length between the samples and the optical signals, resulting in a deep modulation on the optical signal. Moreover, in places of a bulky chamber for hosting liquid/gas samples in conventional fiber-based sensing configurations, the tiny voids in MOFs save the volume of sensing samples and avoid contaminations, making the sensing scheme more compact for in-line sensing applications. In this chapter, we first introduce the structures of MOFs and lightwave guiding mechanisms in MOFs, including index-guiding mechanism, photonic bandgap guiding mechanism, and antiresonance guiding mechanism. Then, we present MOF fabrication methods for different fiber structures and materials. Last but not least, several kinds of MOF-incorporated sensing configurations, including fiber gratings, Fabry–Pérot interferometers, Mach–Zehnder interferometers, and Sagnac interferometers, and surface-enhanced Raman scatterings, are discussed with theoretical analysis and cutting-edge achievements in a few application scenarios.

N. Zhang (✉)
Shenzhen JPT Opto-Electronics Co., Ltd, Tellhow Industrial Park,
Hi-tech Industrial Area, Guanlan Town, Shenzhen 518110, China
e-mail: zhangnan@jptoe.com

G. Humbert
XLIM Research Institute - UMR 7252 CNRS, University of Limoges,
123 Avenue Albert Thomas, Limoges Cedex, France
e-mail: georges.humbert@xlim.fr

Z. Wu
Fujian Key Laboratory of Light Propagation and Transformation,
College of Information Science and Engineering, Huaqiao University,
Xiamen 361021, China
e-mail: zfwu@hqu.edu.cn

Keywords Photonic crystal fibers · PCF fabrication methods · Long period fiber grating · Fiber interferometer · Fiber surface-enhanced Raman scattering sensing

1 Introduction

Optical fiber sensing networks have distinct features of high robustness, immunity to electromagnetic interference, small size, good repeatability, and enabling remote sensing configurations (Consales et al. 2012). In particular, optical fibers are made of silica. It is a dielectric material and has high melt temperature (~1700 °C), making optical fibers immune to the ambient electromagnetic signals and harsh environment. By possessing a small cross section of hundred micrometers and a low transmission loss, optical fibers show great flexibility and benefits in constructing networks for remote sensing applications. Moreover, the advanced fiber fabrication technology leads to good consistency in the fiber geometry over long length and helps to save cost for mass production. Owing to these distinguished features, fiber-based sensing platforms have attracted intensive research and exploration, and rapidly being applied widely from environment monitoring to biological detections.

Conventional single-mode fibers (SMFs) and multimode fibers (MMFs) have a germanium-doped silica fiber core surrounded by a pure-silica cladding. The refractive index (RI) of fiber core is larger than that of fiber cladding, and light guidance in the fiber core relies on total internal reflection (TIR). Though SMFs and MMFs have been successfully applied to temperature (Peng et al. 2016), strain (Zhu et al. 2012), curvature (Mao et al. 2014), and RI (Rong et al. 2012) analysis, the extremely weak light–matter interaction property hampers their spectral response's sensitivity to ambient variations, hence, making the sensing scheme exhibits either low sensing sensitivity or redundant in fiber length. A few techniques have been applied to conventional fibers to enhance light–matter interaction, such as fiber gratings, microbubbles, microfibers, and side-polished fibers. These microstructures on fibers have low fabrication reproducibility and are fragile, causing difficulties in integration and instability of sensing networks. Besides, all-solid fiber geometry requires external chambers for liquid flow, which compromises compactness of the systems.

To address these challenges and enhance light–matter interaction, MOFs are proposed and have been investigated for sensing applications in the past two decades. MOFs, mainly refer to photonic crystal fibers (PCFs), enable light trapping in the solid/hollow fiber core through modified TIR, photonic bandgap (PBG) or antiresonance etc. by the periodic microstructures in the fiber cladding region. The scanning electron microscope (SEM) images of a typical pure-silica solid-core PCF and a PBG fiber are shown in Fig. 1a, b, respectively. Because the main motivation when the idea of PCFs was first proposed was to fabricate a hollow-core fiber that confines light through PBG effect enabled by a cross-sectionally periodic photonic crystal structure, the term PCF was introduced and remains in use for the whole class of microstructured fibers, either with or without any kind of "crystal" structure.
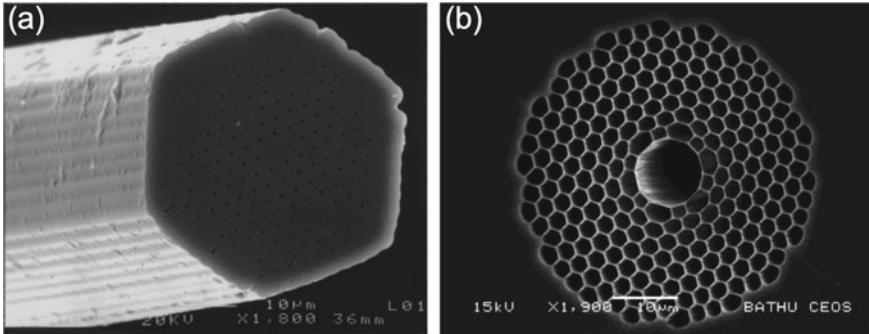
Fig. 1 SEM photograph of **a** the first solid-core index-guiding PCF (Adapted with permission from Knight et al. 1996); and **b** a typical hollow photonic bandgap PCF (Adapted with permission from Lynch-Klarup et al. 2013)

The holey structure of PCFs provides inherent advantages in improving the compactness and performance of fiber-based sensors. In particular, firstly, the air channels can host the liquid/gas media. And, as the air channels generally have a diameter of a few micrometers or tens of micrometers, relatively small sample volume is needed for completing the sensing/detection. Secondly, the large hollow core or the air channels tightly surrounding the solid fiber core enable a large overlap between the sample in the channels and the electrical field of the light beam, thus to dramatically enhance the modulation capability to the light signal, resulting in a better sensing resolution. Thirdly, the unprecedented long effective interaction length enabled by the air channels running along the entire fiber length can contribute to improve the limit of detection in absorption-based sensing configurations. Besides, PCF-based sensors are especially suitable for in-line real-time sensing applications in which the liquid/gas samples continuously flow through the sensing region via inlet and outlet, and the spectrum is recorded and analyzed in real time.

Over the past few decades, the main research interests of PCFs-based sensors has been focused on increasing sensing sensitivity, constructing in-line sensing configurations, and expanding the application scenarios by exploring new PCF structures and integrating other sensing techniques like fiber gratings and interferometers. In terms of exploring new fiber structure, great efforts have been put on enlarging evanescent field in the air channels and easy accessibility of liquid/gas samples to the internal air channels. For example, suspended-core fiber, with 3 larger air channels surrounding a small solid-core region (as shown in Fig. 3a), has been intensively explored for high-sensitivity molecular detection because of its extremely large evanescent power ratio in the air channels. The simple wheel-like structure makes the lateral access of liquid easy as well. The integration with other techniques enables higher sensitivity sensing, and wider application scenarios like RI sensing, or extracting structural fingerprinting information of biological molecules.

In this chapter, we first give a brief introduction to the fundamentals of PCFs, including lightwave guiding mechanisms, the key geometric parameters that affects

its optical properties, and advanced fiber fabrication methods. Then, we will summarize a few most compact and highly sensitive liquid/gas sensing configurations that adopt PCFs, including fiber gratings, fiber interferometers, and surface-enhanced Raman scattering, and their cutting-edge achievements in versatile sensing scenarios.

2 Guiding Mechanisms of PCFs

Lightwave guidance mechanisms in the core region of PCFs are mainly classified as index guiding, PBG guiding, and antiresonance guiding.

- Index guiding

In index-guiding PCFs, light is confined in the core area through modified TIR. TIR is a phenomenon that the total amount of the incident light energy is reflected back at the boundary between two different media. It only occurs when the lightwave travels in a high RI medium approaches the other medium with a lower RI at an angle of incidence larger than the critical angle. Normally, index-guiding PCFs are made of pure silica. The RI difference between the core region and the cladding region is obtained by creating periodic holey structures in the cladding region to reduce the averaged RI of the cladding region. A typical structure of an index-guiding PCF is illustrated in Fig. 2. The presence of air holes decreases the overall RI value of the cladding region, because air has a low RI value (1.0) than that of silica (e.g., 1.444 at the wavelength of 1550 nm). The pitch of the air channels (distance between two adjacent air channels) is represented by symbol Λ, and the diameter of air hole

Fig. 2 A schematic illustration of an index-guiding PCFs made of pure silica. The green color represents the silica material, and the white regions are air
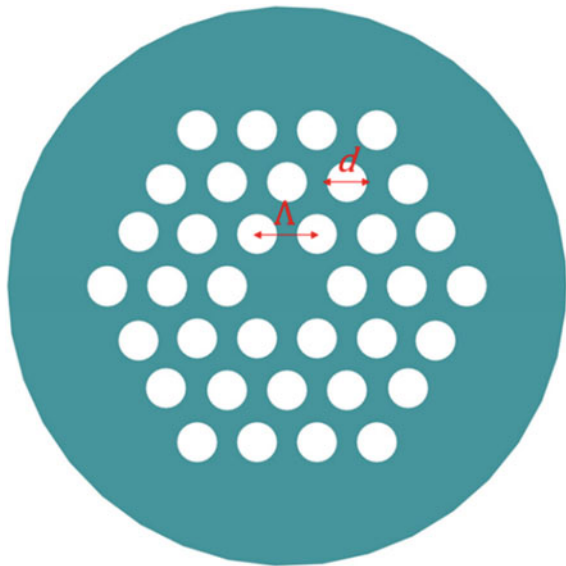
is indicated by d. Simulation results suggest that a smaller pitch and a larger air hole diameter can help to increase the evanescent power fraction in the air channels located in the innermost ring. And, increasing the number of rings helps to reduce the fiber transmission loss.

The mode number analysis of index-guiding PCFs can refer to that of step-index fibers. The number of transverse modes (M) that are supported in the step-index conventional fiber core can be theoretically predicted by the following equations:

$$V = \tfrac{2\pi}{\lambda} a \sqrt{n_{\text{core}}^2 - n_{\text{cladding}}^2} \tag{1}$$

$$M = \tfrac{V^2}{4} \tag{2}$$

where a is the radius of the fiber core, λ is the wavelength of the light wave, and n_{core} and n_{cladding} refer to the RIs of the fiber core and cladding regions, respectively. V number is the normalized frequency parameter. When $V < 2.405$, step-index fibers only support single-mode propagation, which is the fundamental mode. For a typical PCF structure which has periodic air holes in the cladding, the RI of the cladding can be estimated through an effective index model (Knight et al. 1998). In the effective index model, the RI of the cladding is defined according to the propagation constant of the fundamental space-filling mode of the infinite cladding, and d/Λ play an important role in determining the number of modes. An effective V value (V_{eff}) for a PCF can be defined as (Birks et al. 1997; Vengsarkar et al. 1996):

$$V_{\text{eff}} = \tfrac{2\pi}{\lambda} a \sqrt{(n_{\text{core}}^2 - n_{\text{a}}^2)F} \tag{3}$$

where, n_{a} is the RI of air ($n_{\text{a}} = 1$), and $F = d/\Lambda$ is the air filling ratio.

- PBG guiding

There is another kind of PCFs in which the fiber core exhibits a smaller RI than that of the cladding region. Obviously, TIR does not work in this situation. In this kind of PCF, light of a certain band of wavelength is confined in the low index core by the PBG effect of the photonic crystal structure in the cladding region. Therefore, it is categorized as PBG fibers. Usually, PBG effect only guarantees relatively narrow transmission bandwidth. The first hollow-core photonic bandgap structure fiber was fabricated in 1998. However, the guided mode in this fiber was observed to be evanescent in the central air channel. To support stable light propagation in the central air core, numerical calculations reveal that a large air filling ratio and a small pitch in the surrounding photonic crystal cladding structure are necessary (Cregan 1999). Later, in 1999, R. F. Cregan in the University of Bath successfully fabricated the first photonic bandgap guiding fiber that supported single-mode propagation in the air core (Cregan 1999). In this fiber, the large hollow core was obtained by removing 7 capillaries in the center, and the air filling ratio and pitch in the cladding are ~39% and 4.9 μm, respectively. However, the researchers only receive 35% of an input laser energy after propagating through a 4 cm long fiber sample due to low input coupling

efficiency and the scattering loss resulted from surface roughness of the inner ring of cladding. In 2005, an ultimate low-loss photonic bandgap fiber (1.2 dB/km) was obtained by reducing surface roughness (Roberts et al. 2005).

In addition, Bragg fibers and all-solid photonic bandgap fibers are also proposed and investigated for exploring new optical properties. Bragg fibers are usually made of polymer and soft glasses instead of silica. Light is confined in the large hollow core by the surrounding multilayer reflector consist of alternating high index (soft glasses) thin films and low index films (polymers). A Bragg fiber that is used for CO_2 laser beam delivery (Temelkuran et al. 2002) is shown in Fig. 3b.

All-solid photonic bandgap fiber structure is realized by replacing the air holes of index-guiding PCFs with high index material (larger than core), as shown in Fig. 3c. Compared with holey structured PBG fiber, all-solid PBG fibers are easier to fabricate, and it shows better coupling performance especially when splicing with standard SMFs or MMFs.
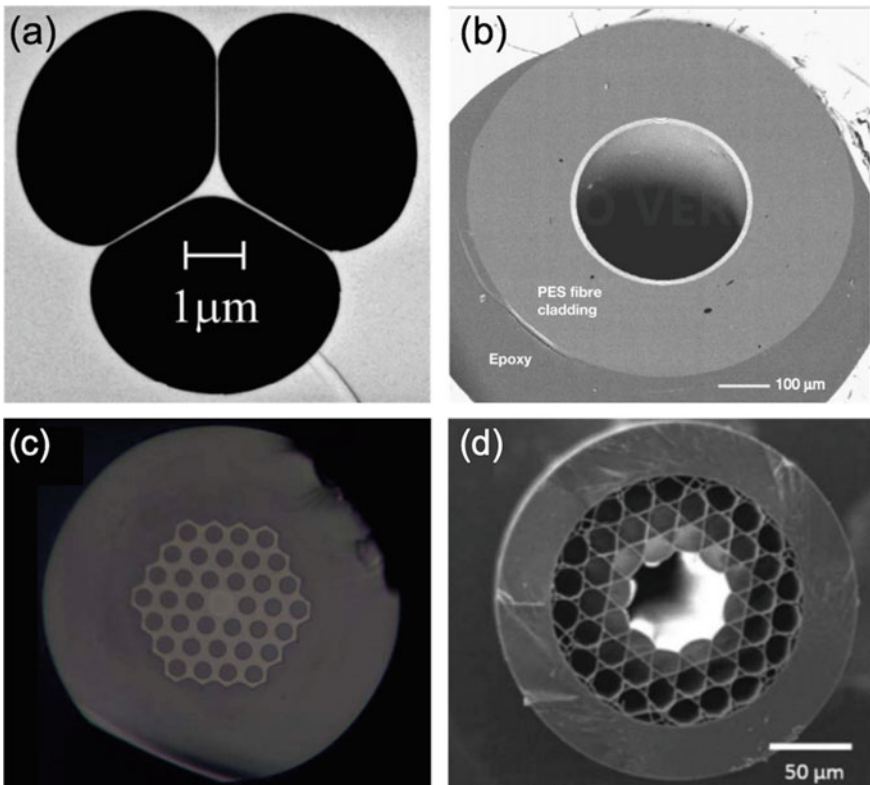

Fig. 3 SEM photograph of **a** a suspended core fiber (Adapted with permission from Monro et al. 2010); **b** a Bragg fiber (Adapted with permission from Temelkuran et al. 2002); **c** all-solid PCF (Adapted with permission from Wang et al. 2015); and **d** Kagome-like hollow-core PCF (Adapted with permission from Subramanian et al. 2017)

- Antiresonance

The first hollow-core PCF capable of transmitting light over a broad range of optical frequencies was demonstrated in 2002 (Benabid et al. 2002). The cladding structure of this fiber consists of thin (nanometer scale) silica webs arranged in a Kagome lattice instead of conventional triangular hollow-core PCF structures reported previously. But numerical simulation reveals that the cladding structure does not support any PBGs. Further research progress on broadband-guiding hollow-core PCF indicates that: 1. The geometry of the cladding is not the crucial factor in exhibiting broadband guidance in the Kagome-like hollow-core PCFs; 2. in contrast to hollow-core PBG fibers, the transmission loss of this kind of fiber is independent of the number of cladding layers; and 3. the geometry of the first silica layer surrounding the hollow core is essential for determining the performance of the broadband-guiding hollow-core PCFs (Markos et al. 2017). There are a few other types of hollow-core PCF structures that support broadband spectrum guidance, such as negative-curvature hollow-core PCFs or single-ring hollow-core PCFs. According to current research, broadband-guiding hollow-core PCFs does not show a unique cladding design and neither has an accepted guidance mechanism. It may be composed of a Kagome-like (Fig. 3d), a honey-comb lattice or a reduced or even single layer of annular tubes (Pryamikov et al. 2011). The guidance mechanisms in broadband-guiding hollow-core PCFs are also still a subject of study or debate, commonly perceived as inhibited-coupling or antiresonance guiding.

3 PCF Fabrication Technology

The fabrication of PCFs is proved far from easy. It took a long journey to succeed until the year of 1996 when Prof. J. C. Knight and his colleagues reported that they successfully fabricated the first silica-air PCF in the University of Southampton by means of capillaries stacking (Knight et al. 1996). This PCF has a solid core surrounded by periodic air arrays in the cladding region, and it confines light through TIR (index guiding) the same as the conventional SMFs and MMFs. Soon after, with the successful experience of fabricating index-guiding PCFs, the first PBG PCF was achieved in 1998.

The fabrication process of a fiber normally involves two basic steps: preform preparation and drawing process with a fiber drawing tower. The preform has the same structure and RI profile as the final fiber sample, but larger in size. The diameter of the cross section of a fiber preform is around a few centimeters.

Depending on different fiber structures and materials, a few techniques have been practiced to prepare the large fiber preform, such as stacking (Russell 2003), extrusion (Kumar et al. 2002), and rolling (Temelkuran et al. 2002).
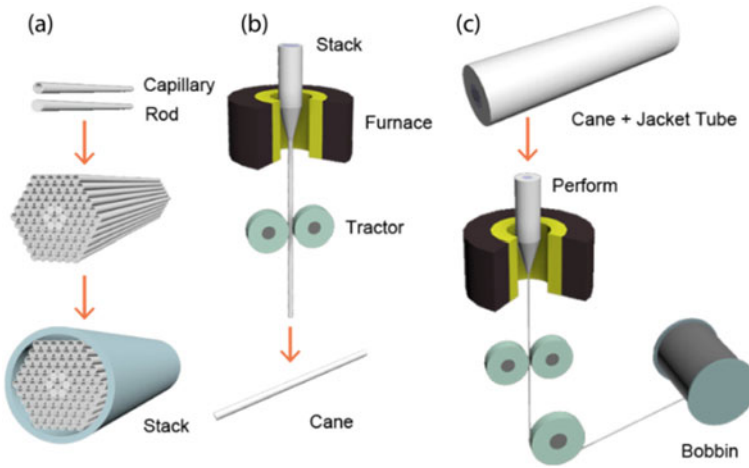
- Stack-and-draw method

Fig. 4 A brief schematic diagram of stack-and-draw method for the fabrication of PCFs. **a** Assembling silica capillaries and rods into macroscopic preform stack. **b** The large preform stack is drawn into canes with a diameter of a few millimeters. **c** The final thermal draw step to achieve PCFs with a diameter of a few hundred micrometers (Adapted with permission from Ma et al. 2017)

In terms of fabricating silica PCFs preform, the most commonly used method is capillary/rod stacking. Capillaries are small silica tubes that have the same air filling ratio with that of the PCF cladding region. They are generally 1 m long with an outer diameter of a few millimeters and obtained from drawing large silica tube/rods. For preparing a preform with stacking method, first, capillaries and rods are stacked following the designed photonic crystal pattern. Then, the stack is inserted into a larger silica tube to provide an outer protecting silica layer. Next, the preform will be mounted in the preform holder on the top of a fiber drawing tower and drawn to be thinner cans/fibers when fed into a high-temperature furnace (operating at above 1700 °C). Figure 4 shows the procedure of a fiber drawing process.

Because the thermal expansion coefficients of silica and air are quite different and the draw-down ratio from the preform to fiber is large, to prevent the breaking of preform or damage of the fiber structure, the complete drawing process normally involves two steps:

1. Feed the preform into the high-temperature furnace and achieve a smaller-sized cane which has an outer diameter of a few millimeters.
2. Feed the cane into the furnace again and draw to obtain regular fibers following adding an extra silica jacket to achieve thicker outer cladding region.

To obtain a perfect fiber structure, the drawing process is very challenging. The feeding speed (speed of the preform/cane, V_{seed}) and drawing speed (speed of the fiber, V_{fiber}) of the preform together determine the draw-down ratio of the drawing process by the following relationship:

$$V_{\text{seed}} R_{\text{seed}}^2 = V_{\text{fiber}} R_{\text{fiber}}^2 \tag{4}$$

where R_{seed} and R_{fiber} are the radii of the seed preform/cane and the produced cane/fiber, respectively. Moreover, to perfectly maintain the fiber structure, the furnace temperature, the pressure in the air channels, and vacuum environment in some circumstances need to be precisely managed. In particular, for holey structured PCFs, when the temperature goes too high, the air in the channels expand rapidly and may destroy the thin silica webs in the microstructure. Inversely, the fiber is easy to break in a low temperature applied. The temperature applied to the preform/cane is crucial. It relies on both of the temperature of furnace and the feeding speed of the preform as fast feeding speed reduce heat accumulation in the fiber. The pressure applied in the air channel helps to maintain the fiber structure, and the vacuum applied to the preform tube in some circumstances is intended to suppress the interstitial holes in the joints of silica web.

Therefore, to obtain a fine fiber structure, those parameters including furnace temperature, the pressure applied, feeding speed of preform, and drawing speed need to be precisely adjusted. And this requires a few rounds of trials and improvements. Besides, the large surface area of capillaries and rods in the preform stack could introduce contamination easily. But this method of making preform allows large flexibility in fiber structure design.

- Extrusion

Extrusion method can be applied to realize silica-air preforms that are not readily achievable by stacking capillaries and rods. In the preform fabrication process, a molten glass is penetrated through by a die having the desired patterns of holes. Therefore, it is especially suitable for fabricating fiber preform made of low melting temperature materials, for example, chalcogenide glass, polymers, or those materials which are not readily available in tube form. Then, the bulky glass preform is drawn using a thermal-drawing tower which is the same to the one shown in Fig. 4b. This kind of fabrication method allows the fabrications of any regular or irregular structured fibers. The first non-silica glass PCF using extrusion method is made of glass SF57 (Kiang et al. 2002). It exhibits a "wheel"-like structure with 3 large air channels surrounding a small solid core, and observed to be single mode over a broad wavelength range.

Extrusion provides a controlled and reproducible method for fabricating holey preform with complex structure and good surface quality. By broadening the applicable range of materials and structure designs, extruded holey fibers offer a wider range of optical properties compared with the stacking method. Moreover, as fewer interfaces are involved, extrusion shows the potential to minimize the ultimate transmission loss by avoiding contamination.

- Rolling method

Rolling is perfectly suitable for the fabrication of fiber with periodic annular layers structure, like Bragg fibers or omnidirectional fibers. In this method, multilayers

of polymer-based mirrors are rolled up to present a preform with a hollow core and alternate high refractive index and low index in the cladding region. The index variation in the radial direction provides the light guidance capability in the hollow fore region through photonic bandgap mechanism.

This method is widely used in fabricating preform that combines polymer and glass materials (Temelkuran et al. 2002). And the wavelength scalability (the control over transmission band through the fiber's geometrical parameters) is available by changing the thickness of the thin layers. A. M. Stolyarov et al. demonstrated an omni-directional PBG fiber that confines the visible wavelength for trace vapor sensing (Stolyarov et al. 2012). This fiber was thermally drawn from a preform comprised of 15 bilayers of chalcogenide glass (As_2S_3) and polyetherimide (PEI) and a cladding made of PEI.

4   Processing for in-Line Access

The in-line accessibility to the PCF channels is important for prompting the use of PCF for sensing applications. Because it speeds up getting sensing results, ensures the reusability of fiber samples, and also eliminates the measurement error introduce when realign a new fiber sample. A considerable part of PCF-based in-line sensing configuration is constructed in this form that: The light beam is coupled into the fiber core through precise position alignment (free space coupling), while both of the PCF fiber ends are housed by microfluidic reservoirs, as illustrated in Fig. 5a. The liquid flow through the PCFs is forced to continue by the pressure difference between the two reservoirs. In this way, simultaneous liquid flow in all the air channels of PCF and light coupling to the fiber core are realized. This configuration can also be applied to selective liquid filling into the air channels in PCFs, with a pretreatment to block the rest of the air channels. However, the precise free space light coupling requires high mechanical robustness and might be subject to the pressure perturbation in the microfluidic reservoir. There is another attempt to insert and splice a 20-μm-width C-shaped fiber between the PCF and SMFs to create liquid inlet and outlet, as shown in Fig. 5b. The splicing connection is much more robust, but this method requires precise manipulation on very tiny C-shaped fiber, which is difficult. Besides, laser micromachining or coupled with hydrogen fluoride (HF) etching can drill a hole from the side of the PCF to enable the liquid flow into the air channels. This method makes it possible to choose any drilling positions, but it may destroy the fiber structure, introduce contamination, and most importantly only the outer rings of air channels are accessible.

In addition to the post-processing methods, researchers also have proposed novel fiber structures to enable convenient liquid access to the air channels in PCFs. In 2011, H. W. Lee et al. in Prof. P. Russell's group proposed a step-index fiber with a parallel hollow micro-channel (Lee et al. 2011) to provide convenient liquid insertion and avoid complex selective channel introduction process. Also, a side-channel PCF (SC-PCF) is proposed to provide easy access to the lateral large side channel and
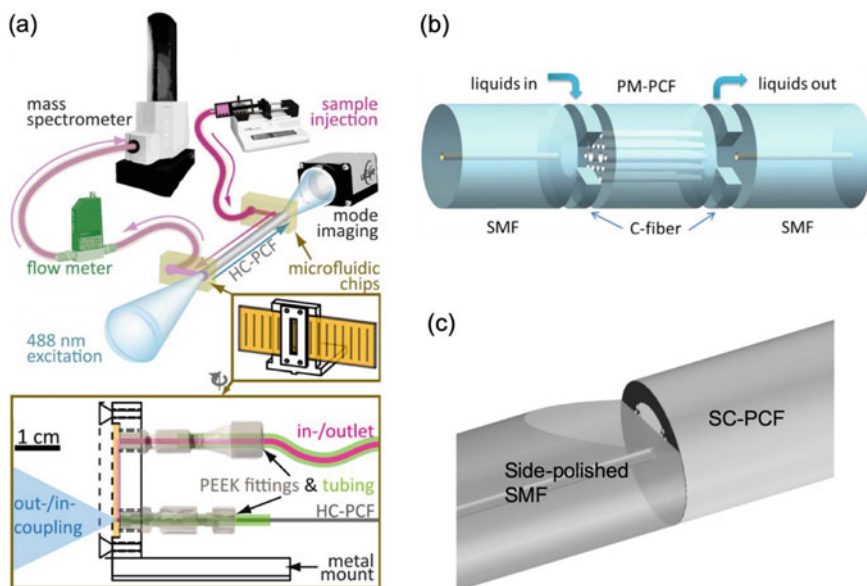
Fig. 5 A schematic diagram showing the methods to enable simultaneous light coupling and in-line liquid access to PCFs: **a** free space coupling (Adapted with permission from Unterkofler et al. 2012); **b** inserting a C-shaped fiber between SMF and PCF (Adapted with permission from Wu et al. 2013); and **c** splicing the SC-PCF to side-polished SMF (Adapted with permission from Zhang et al. 2016a, b)

large evanescent power in the side channel for improving sensing performance. The structure of SC-PCF is elaborately designed to have a larger channel in one side of the PCF, so that the simultaneous light coupling and liquid access can be enabled through splicing it with a side-polished SMF (as shown in Fig. 5c). The side-polished SMF is manufactured by polishing a glass cuboid with a bare SMF buried in its groove with wax, and its produced geometric parameters are well designed to expose the side channel to the external environment only.

5 Sensing Applications

PCF-based fiber sensing configurations have been applied to physical sensing, chemical sensing, and biomedical sensing, owing to its diversity in optical waveguide properties. Among these, aqueous sensing is particularly attractive as the voids in PCF are natural liquid carrier. The analysis of aqueous/gaseous samples can be done through tracing a few parameters: absorption loss of light beam it introduced, RI, photoluminescence phenomenon, Raman spectrum, etc. Measuring the RI of aqueous sample is a very important method to analyze the presence of analytes in

the aqueous solutions and its concentrations. It is a label-free detection method and is easy to implement and commonly realized through monitoring the resonant wavelength shift of a long period grating (LPG) or interferometry since the RI of liquid in the sensing region has an impact on the effective refractive index (ERI) of the transverse modes and the distribution of the modal energy. With the increasing demands of specific detection of chemical and biological molecules, some researchers have explored specific detection on DNA or RNAs by adding preparations on fiber/core surface in RI sensors. Another technique, surface enhance Raman scattering (SERS), also has attracted large interests, for its capability of revealing fingerprinting information of the molecule with high sensitivity by directly analyzing the Raman spectrum collected from the fiber ends.

In this section, we will focus on LPG fiber sensors and interferometric fiber sensors, as well as SERS fiber sensors which particularly interest the current research and also make up a large proportion of PCF based sensors.

• Long period gratings fiber sensors

LPG is a structure of periodic RI variation along the fiber axial direction. The structure has a period in the sub-millimeter scale and is able to realize mode energy coupling between two co-propagating transverse modes at a certain resonant wavelength (λ_{res}) when satisfy the phase matching condition:

$$n_{eff}^1 - n_{eff}^n = \frac{\lambda_{res}}{\delta} \tag{5}$$

where, n_{eff}^1 and n_{eff}^n are the ERIs of the coupling transverse modes. δ is the pitch of the grating structure. Therefore, if a gating pitch has been chosen to realize the energy coupling from fundamental mode to higher-order core mode or cladding modes, there will be a series of low power bands in the transmission spectrum as high-order modes experience larger transmission loss.

According to Eq. (5), we can clearly see that with a certain pitch, the resonant dips are dependent on the difference between the ERIs of the two coupling modes which can be affected by the RI of liquid filling in the channels of PCFs. In this way, the variation in the RI of the liquid sample can be monitored through tracing the shift of LPG dip wavelength.

Fiber LPGs can be fabricated through several methods, for example, point-by-point laser writing method (Wang et al. 2006), mechanical pressure (Hu et al. 2012a, b), and electric arc technique (Humbert et al. 2003). Among of these, CO_2 laser point-by-point imprinting method is the most commonly used one. The CO_2 laser irradiation imposes thermal effect on fiber surface and can affect the RI of the PCF via three mechanisms:

1. Release stress introduced during the fiber fabrication process
2. Cause slight deformation on the fiber surface
3. Introduce stretch force when heating up the silica fiber.

With the combination of a computer-controlled precise moving stage, CO_2 laser point-by-point imprinting method enables great flexibility in fabricating LPGs with

different pitch, grating numbers, and writing position to control over the modulation depth and resonant wavelength of the LPGs. The grating obtained with laser inscription is permanent, so it can be established for long time and stable sensing applications.

PCF LPGs sensing configurations provide reliable RI measurements with high sensitivity. Attempts have been made to inscribe LPG on various kinds of PCFs. It is reported that fiber gratings on the large-mode-area PCF are able to deliver a high RI sensitivity of 1500 nm/RIU near a RI value close to water (1.33), which is nearly 2 order of magnitude higher than that can be obtained with SMF LPG (Rindorf and Bang 2008). In this work, the authors fabricate an LPG on a large-mode-area PCF which has a solid core and an air channel lattice cladding with the pitch and the ratio of air hole diameter to pitch being 7.12 μm and 0.478, respectively. The resonance occurs at the wavelength of 1050 nm with a grating period of 580 μm and period number of 60. The RI sensitivity is characterized by tracing the blue shift amount of the resonant wavelength when tuning the RI of the methanol solution infiltrated in the channels through temperature.

In-line access of liquid into the air channels of PCF LPGs enables direct measurements of RI sensitivity through dynamic liquid infiltration. An LPG inscribe on a side-channel PCF (SC-PCF) designed to enable direct and highly sensitive RI measurement (Zhang et al. 2016a, b). The SC-PCF enables a large side channel adjacent to the solid core for fast liquid infiltration of the test sample and large evanescent power. The LPG on SC-PCF has a grating period of 153 μm and a period number of 50, resulting in the modal energy coupling between LP_{01} and LP_{11} mode. The resonance dip in the transmission spectrum is centered at 1520 nm with a full bandwidth at half maximum (FWHM) of ~21 nm and an extinction ratio of ~7 dB. The RI sensitivity is characterized to be 1145 nm/RIU over the RI range of 1.3330–1.3961 through the infiltration of RI solutions (sodium chloride solutions with different concentrations) into the large side channel adjacent to the solid core. This continuous-flow configuration makes this sensing platform very promising for real-time monitoring.

In addition to non-specific RI sensing, PCF-based LPG sensors are also reported for specific biological sensing application. In 2006, L. Rindorf et al. demonstrated the use of a PCF LPG to detect the thickness of poly-L-lysine and double-stranded DNA immobilized on the inner wall of the air channels through electrostatic (Rindorf et al. 2006). Because the test molecules are deposited on the side of the holes where they interact with intense evanescent wave, the sensor is regarded more robust to environmental temperature variation and the influence of the liquid in the air holes. In 2011, Z. He et al. reported an endless single-mode PCF LPG sensor that realized specific goat anti-mouse IgG (H + L) antibodies. It, for the first time, realized a PCF LPG that carry out multilayer biomolecular binding events in the air channel of PCF cladding (He et al. 2011) and each step of binding event on the wall of channels cam be monitored through the shift of LPG resonant wavelength. Though the sensing/detection of biomolecules with fiber LPGs is essentially attributed to the modulation of sample RI to the resonant wavelength, immobilization of multilayer biomolecular binding method eliminates the perturbation from other molecules.

PCF LPG sensors are compact in configuration and offer relatively high sensitivity. Taking advantages of the liquid voids in PCF, it is very promising in serving as a platform for real-time and online measurements, as well as for biological and chemical sensing which may require multilayer treatment on the silica surface for specific identification.

- Interferometer sensors

In optical fibers, interference between two propagation modes can be realized in a single fiber or in two separate fibers as long as the two modes travel over different optical paths. Assume the two interference beams are split from a single beam, which means that there is no phase difference at the very beginning. After passing through different optical paths, the recombined output intensity I can be predicted by the following equation:

$$I = I_1 + I_2 + 2\sqrt{I_1 I_2} \cos(\Delta\psi) \tag{6}$$

$$\Delta\psi = \tfrac{2\pi}{\lambda}(n_1 l_1 - n_2 l_2) \tag{7}$$

where I_1 and I_2 are the intensities of the two interference beams at the position of recombination, respectively. n_1, l_1 and n_2, l_2 are ERIs of the two modes and the fiber lengths they pass through. $\Delta\psi$ represents the optical phase difference (OPD) between the two beams, and λ is the wavelength. From the equation, we can identify that the output intensity shows periodic resonant dips/peaks in the transmission spectrum. Because OPD is relevant to ERIs of the propagation modes, the resonance dips will shift in response to the RI variation in the sensing region.

PCF-based interferometric RI sensing configurations includes Fabry–Pérot interferometers (FPI), Mach–Zehnder interferometers (MZI), and Sagnac interferometer (SI). In particular, a concave-core PCF constructed FPI sensor is reported to exhibit an RI sensitivity of 1635.62 nm/RIU (Tian et al. 2016). The FP sensor is built by splicing a segment of concave-core PCF with a SMF, and the shallow concave-core of the fiber form the FP cavity directly. J. J. Hu et al. demonstrate a highly sensitive PCF MZI by splicing both ends of a PCF with SMFs using fusion arc splicing technique. The air channels of the PCF are completely collapsed in both splicing region, serving as beam splitter and beam combiner to excite mode coupling to/from high-order cladding modes (Hu et al. 2012a, b). Since the evanescent field of the high-order cladding mode extends to the external medium, the RI of the external medium affects the ERI of the cladding mode, whereas not that of the core modes. The RI variation will induce OPD change and lead to variation in the transmission spectrum. The RI sensitivity was demonstrated to be 320 nm/RIU over the biosensing RI range (1.33–1.34) by immersing the PCF in different RI solutions. In 2013, T. Han et al. reported a selective-filling PCF-based Sagnac interferometer (Han et al. 2013). The two channels in the innermost ring of the fiber cladding are selectively filled

with liquids that has a higher RI index than silica to guide light by a combination of index-guiding and bandgap guiding. It is characterized to enable an RI sensitivity of 63,882 nm/RIU by heating the fiber with a temperature chamber. C. Wu reports an in-line optofluidic polarization maintaining PCF-based SI sensor. It allows simultaneous light injection into the fiber core and liquids flow in and out by inserting C-shaped fibers between PCF and SMFs (Wu et al. 2014). The schematic diagram is shown in Fig. 5b. By changing the RI solutions (sodium chloride solutions) that flows through the fiber from the opening, its RI sensitivity is measured to be 8699 nm/RIU.

In 2018, N. Zhang et al. presented a side-channel PCF SI for ultra-sensitive chemical and biological analysis (Zhang et al. 2018). The geometry of the side-channel PCF is shown in Fig. 6a. To increase the fraction of evanescent power in the large side channel and maintain a relatively small insertion loss when spliced with SMFs, the pitch and the ratio of air hole diameter to the pitch are fabricated to be 6 μm and 0.6, respectively. To enable lateral liquid access to the large side channel for the convenience of liquid flow in and out, the side-channel PCF is spliced with a side-polished SMF to create an opening. The sensing scheme is constructed in this way to support specific chemical and biological analysis that require multilayer treatments on the silica surface. Figure 6c shows the resonance in the transmission spectra when the side channel is empty and filled with water. RI sensitivity is measured to be 2849 nm/RIU. Specific sensing performance with side-channel PCF Sagnac interferometer is characterized using human cardiac troponin T (cTnT) protein detection.
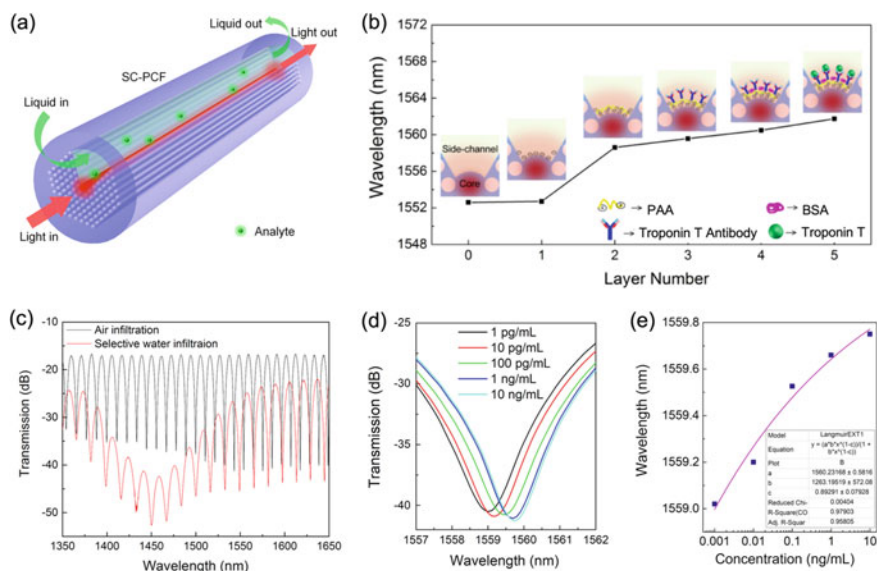

Fig. 6 a Schematic diagram of the sensing configuration; **b** resonance dips recorded along with the multilayer deposition; **c** transmission spectrum of the side-channel PCF interferometer; **d** resonant wavelength shift corresponding to different antibody concentration, and **e** their correlation relationship (Zhang et al. 2018). Reproduced by permission of The Royal Society of Chemistry

Specific cTnT detection needs a series immobilization of OH$^-$ group, a monolayer of poly(allylamine), active cTnT antibody, and cTnT antibody in sequence. Before each immobilization step, distilled water or phosphate-buffered saline (PBS) is used to rinse the residuals from the previous step. And resonance wavelength variations are recorded in real time after each binding step of the layers, as recorded in Fig. 6b. Eventually, cTnT solutions are infiltrated in an ascending order of concentration from 1 pg/mL, and the shift of resonance dips is plotted in Fig. 6d, e, revealing a limit of detection of 1 ng/mL.

Overall, PCF-based interferometers exhibit characteristics of easy fabrication, simple structures, high integration level, and high sensitivity. Similar to PCF-based LPG sensors, they deliver a highly efficient solution to chemical and biological analysis for environmental monitoring or biological/medical diagnosis.

- Surface-enhanced Raman scattering sensing

Raman spectrum reveals the information of a molecule in vibrational mode level which relies on the molecule's constituent atoms, chemical bind strengths, and their structural arrangements. As each kind of molecules has its unique structures, the Raman spectrum is specific to one kind of molecules. Surface-enhanced Raman scattering (SERS) is a technique that amplifies Raman signal of the molecules thus to dramatically improve the limit of detection of test molecules. This amplification is realized by an intense electromagnetic field on a roughed noble metal surface that stems from the excitation of certain special coupling of surface plasmon. The intensity of SERS signal ($P^{\mathrm{SERS}}(\upsilon_{\mathrm{S}})$) obeys the following equation:

$$P^{\mathrm{SERS}}(\upsilon_{\mathrm{S}}) = N' \cdot \sigma_{\mathrm{inc}}^{\mathrm{R}} \cdot |A(\upsilon_{\mathrm{L}})|^2 \cdot |A(\upsilon_{\mathrm{S}})|^2 \cdot I(\upsilon_{\mathrm{L}}) \tag{8}$$

where $A(\upsilon_{\mathrm{L}})$ and $A(\upsilon_{\mathrm{S}})$ are the enhancement factors of excitation laser electromagnetic field and scattered Raman electromagnetic field, respectively. $\sigma_{\mathrm{inc}}^{\mathrm{R}}$ is the effective Raman cross section. N' is the total number of the molecule that contribute to the Raman signal. $I(\upsilon_{\mathrm{L}})$ is the intensity of excitation laser. SERS is a label-free method that can identify the test molecules with its fingerprinting information; thus, it has attracted large interest in sensing applications with both index-guiding PCFs and bandgap guiding PCFs.

The performance of PCF-based SERS sensors is largely affected by the fiber structure and morphology of the noble metals. In particular, fiber structure affects mode-field overlap in the air channels and minimum confinement loss of the guided modes, and the morphology of the noble metal determines the enhancement factor of both excitation laser electromagnetic field and the scattered Raman electromagnetic field. Compared with solid-core index-guiding PCFs, hollow-core PCFs can obtain Raman signals with low silica background, because the laser beam directly interacts with analyte in the hollow core where both excitation laser and Raman signal are guided. But the narrow transmission window coming along with the bandgap confinement hinders their use in broad Raman scattering spectra.
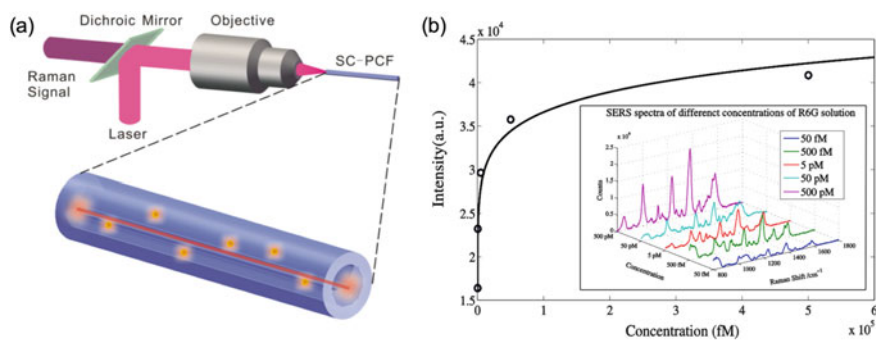
Fig. 7 a Schematic diagram of backscattered SERS sensing scheme. **b** The Raman signal intensity corresponding to the R6G concentration (Zhang et al. 2016a, b)

K. Khaing Oo et al. compared a few PCF structures for SERS applications, including nonlinearity PCFs, steering-wheel PCFs, and suspended-core PCF. The experimental results suggest that the PCF microstructure has a significant effect on the evanescent wave-based sensing and detection (Khaing Oo et al. 2010). And a best limit of detection of 10^{-10} M Rhodamine 6G is achieved with the suspended-core fiber which exhibits the largest fraction of evanescent power in the sensing region. In the experiments, the gold nanoparticles are immobilized on the silica surface of the cladding air channels to provide electromagnetic field amplification. In 2016, the geometry of a side-channel PCF was well defined for SERS sensing applications. The fiber geometry enables large evanescent power in the air channels adjacent to the solid fiber core and a low transmission loss at the SERS excitation wavelength of 632.8 nm with a pitch of 3 μm and an air holes diameter of 2.8 μm in the cladding region. For the SERS measurements, the schematic diagram is shown in Fig. 7a. The excitation laser source at 632.8 nm is coupled into the fiber core from one end of the fiber, and the backscattered enhanced Raman signal is collected and analyzed from the same fiber end. Both the performance under full-filling and selective-filling of the air channels conditions are characterized with a mixture solution of gold nanoparticles and Rhodamine 6G molecule infiltrated. The full-filing configuration reveals a better limit of detection of 50 fM Rhodamine 6G solution. The intensity of the SERS signal under full-filling configuration is plotted in Fig. 7b. In addition, the accumulative phenomenon of Raman signal along the SERS-active fiber length is also investigated, suggesting that properly increasing fiber length is an effective way to further enhance the SERS intensity and thus further reduce the limit of detection.

Compared with conventional fiber-based and substrate-based counterparts, of which the performance is limited by small SERS-active region and weak excitation electromagnetic field in the sensing region, PCF-based SERS sensing platform shows great potentials in constructing high-performance SERS sensing system. By synergistically enabling flexible design of optical waveguide properties and liquid transmission cell in a single fiber, PCFs can contribute to reaching ultra-low limit of

detection and more opportunities for diverse and high-performance sensing applications, such as single molecular detection on cells and clinical diagnosis in liquid samples like urine and blood.

6 Conclusion

In this chapter, we focus on microstructured fibers for sensing applications. By manipulating the materials and fiber structures, light propagation in the PCF fiber core can be realized through index-guiding mechanism, PBG guiding mechanism, and antiresonance guiding mechanism. Coupled with advanced fiber fabrication technology, it allows great flexibility in the design of optical waveguide properties for versatile sensing applications. Hollow-core photonic bandgap fibers offer extremely large mode-field-overlap, but the light transmission loss induced by scattering by liquid is relatively high and the transmission window is relatively narrow. Though, in solid-core index-guiding fibers, the proportion of the evanescent field that extends to the sensing channels is relatively small, it exhibits stable light transmission window and low transmission loss which benefit a stable, robust platform for wide range applications. LPGs, interferometers, and SERS sensing platforms that take advantages of PCF properties show great potentials in in-line and real-time liquid RI sensing, specific chemical and biological molecule identification.

References

F. Benabid, J.C. Knight, G. Antonopoulos, P.S.J. Russell, Stimulated Raman scattering in hydrogen-filled hollow-core photonic crystal fiber. Science **298**(5592), 399–402 (2002). https://doi.org/10.1126/science.1076408

T.A. Birks, J.C. Knight, P.S. Russell, Endlessly single-mode photonic crystal fiber. Opt. Lett. **22**(13), 961–963 (1997). http://doi.org/10.1364/OL.22.000961

M. Consales, M. Pisco, A. Cusano, Lab-on-fiber technology: a new avenue for optical nanosensors. Photonic Sens. **2**(4), 289–314 (2012). https://doi.org/10.1007/s13320-012-0095-y

R.F. Cregan, Single-mode photonic band gap guidance of light in air. Science **285**(5433), 1537–1539 (1999). https://doi.org/10.1126/science.285.5433.1537

T. Han, Y. Liu, Z. Wang, J. Guo, Z. Wu, S. Wang et al., Unique characteristics of a selective-filling photonic crystal fiber Sagnac interferometer and its application as high sensitivity sensor. Opt. Express **21**(1), 122–128 (2013). https://doi.org/10.1364/OE.21.000122

Z. He, F. Tian, Y. Zhu, N. Lavlinskaia, H. Du, Long-period gratings in photonic crystal fiber as an optofluidic label-free biosensor. Biosens. Bioelectron. **26**(12), 4774–4778 (2011). https://doi.org/10.1016/j.bios.2011.05.048

D.J.J. Hu, J.L. Lim, M. Jiang, Y. Wang, F. Luan, P.P. Shum et al., Long period grating cascaded to photonic crystal fiber modal interferometer for simultaneous measurement of temperature and refractive index. Opt. Lett. **37**(12), 2283–2285 (2012a). https://doi.org/10.1364/OL.37.002283

D.J.J. Hu, J.L. Lim, M.K. Park, L.T.H. Kao, Y. Wang, H. Wei, W. Tong, Photonic crystal fiber-based interferometric biosensor for streptavidin and biotin detection. IEEE J. Sel. Top. Quantum Electron. **18**(4), 1293–1297 (2012b). https://doi.org/10.1109/JSTQE.2011.2169492

G. Humbert, A. Malki, S. Février, P. Roy, J.L. Auguste, J.M. Blondy, Long period grating filters fabricated with electric arc in dual concentric core fibers. Opt. Commun. **225**, 47–53 (2003). https://doi.org/10.1016/j.optcom.2003.07.007

M.K. Khaing Oo, Y. Han, J. Kanka, S. Sukhishvili, H. Du, Structure fits the purpose: photonic crystal fibers for evanescent-field surface-enhanced Raman spectroscopy. Opt. Lett. **35**(4), 466–468 (2010). https://doi.org/10.1364/OL.35.000466

K.M. Kiang, K. Frampton, T.M. Monro, R. Moore, J. Tucknott, D.W. Hewak et al., Extruded singlemode non-silica glass holey optical fibres. Electron. Lett. **38**(12), 546 (2002). https://doi.org/10.1049/el:20020421

J.C. Knight, T.A. Birks, P.S.J. Russell, D.M. Atkin, All-silica signal-mode optical fiber with photonic crystal cladding. Opt. Lett. **21**(19), 1547–1549 (1996)

J.C. Knight, T.A. Birks, P.S.J. Russell, J.P. de Sandro, Properties of photonic crystal fiber and the effective index model. **15**(3), 748–752 (1998). https://doi.org/10.1364/JOSAA.15.000748

V.V.R. Kumar, A. George, W. Reeves, J. Knight, P. Russell, F. Omenetto, A. Taylor, Extruded soft glass photonic crystal fiber for ultrabroad supercontinuum generation. Opt. Express **10**(25), 1520–1525 (2002). https://doi.org/10.1364/OE.10.001520

H.W. Lee, M.A. Schmidt, P. Uebel, H. Tyagi, N.Y. Joly, M. Scharrer, P.S.J. Russell, Optofluidic refractive-index sensor in step-index fiber with parallel hollow micro-channel. Opt. Express **19**(9), 8200–8207 (2011). https://doi.org/10.1364/OE.19.008200

K.E. Lynch-Klarup, E.D. Mondloch, M.G. Raymer, D. Arrestier, F. Gerome, F. Benabid, Supercritical xenon-filled hollow-core photonic bandgap fiber. Opt. Express **21**(11), 13726 (2013). https://doi.org/10.1364/OE.21.013726

J. Ma, H.H. Yu, X. Jiang, D.S. Jiang, High-performance temperature sensing using a selectively filled solid-core photonic crystal fiber with a central air-bore. Opt. Express **25**(8), 9406 (2017). https://doi.org/10.1364/oe.25.009406

L. Mao, P. Lu, Z. Lao, D. Liu, J. Zhang, Highly sensitive curvature sensor based on single-mode fiber using core-offset splicing. Opt. Laser Technol. **57**, 39–43 (2014). https://doi.org/10.1016/j.optlastec.2013.09.036

C. Markos, J.C. Travers, A. Abdolvand, B.J. Eggleton, O. Bang, Hybrid photonic-crystal fiber. Rev. Mod. Phys. **89**(4), 1–55 (2017). https://doi.org/10.1103/RevModPhys.89.045003

T.M. Monro, S. Warren-Smith, E.P. Schartner, A. Franois, S. Heng, H. Ebendorff-Heidepriem, S. Afshar, Sensing with suspended-core optical fibers. Opt. Fiber Technol. **16**(6), 343–356 (2010). https://doi.org/10.1016/j.yofte.2010.09.010

Z. Peng, L. Wang, H. Yan, Research on high-temperature sensing characteristics based on modular interference of single-mode multimode single-mode fiber, in *Proceedings of SPIE*, vol. 10025, ed. by T. Liu, S. Jiang, R. Landgraf (2016), p. 1002519. https://doi.org/10.1117/12.2245525

A.D. Pryamikov, A.S. Biriukov, A.F. Kosolapov, V.G. Plotnichenko, S.L. Semjonov, E.M. Dianov, Demonstration of a waveguide regime for a silica hollow-core microstructured optical fiber with a negative curvature of the core boundary in the spectral region >3.5 µm. Opt. Express **19**(2), 1441 (2011). https://doi.org/10.1364/OE.19.001441

L. Rindorf, O. Bang, Highly sensitive refractometer with a photonic-crystal-fiber long-period grating. Opt. Lett. **33**(6), 563–565 (2008). https://doi.org/10.1364/OL.33.000563

L. Rindorf, J.B. Jensen, M. Dufva, L.H. Pedersen, P.E. Høiby, O. Bang, Photonic crystal fiber long-period gratings for biochemical sensing. Opt. Express **14**(18), 8224–8231 (2006). https://doi.org/10.1364/OE.14.008224

P.J. Roberts, F. Couny, H. Sabert, B.J. Mangan, D.P. Williams, L. Farr et al., Ultimate low loss of hollow-core photonic crystal fibres. Opt. Express **13**(1), 236–244 (2005). https://doi.org/10.1364/OPEX.13.000236

Q. Rong, X. Qiao, R. Wang, H. Sun, M. Hu, Z. Feng, High-sensitive fiber-optic refractometer based on a core-diameter-mismatch mach-zehnder interferometer. IEEE Sens. J. **12**(7), 2501–2505 (2012). https://doi.org/10.1109/JSEN.2012.2194700

P. Russell, Photonic crystal fibers. Science **299**(5605), 358–362 (2003). https://doi.org/10.1126/science.1079280

A.M. Stolyarov, A. Gumennik, W. McDaniel, O. Shapira, B. Schell, F. Sorin et al., Enhanced chemiluminescent detection scheme for trace vapor sensing in pneumatically-tuned hollow core photonic bandgap fibers. Opt. Express **20**(11), 12407 (2012). https://doi.org/10.1364/OE.20.012407

K. Subramanian, I. Gabay, A. Shadfan, M. Pawlowski, Y. Wang, T. Tkaczyk, A. Ben-Yakar, A Kagome fiber-based, high energy delivery laser scalpel system for ultrafast laser microsurgery, in *2016 Conference on Lasers and Electro-Optics, CLEO 2016*, vol. 10066, ed. by T.P. Ryan (2017), p. 100660U. https://doi.org/10.1117/12.2253446

B. Temelkuran, S.D. Hart, G. Benoit, J.D. Joannopoulos, Y. Fink, Wavelength-scalable hollow optical fibres with large photonic bandgaps for CO_2 laser transmission. Nature **420**, 650–653 (2002). https://doi.org/10.1038/nature01275

J. Tian, Z. Lu, M. Quan, Y. Jiao, Y. Yao, Fast response Fabry-Perot interferometer microfluidic refractive index fiber sensor based on concave-core photonic crystal fiber. Opt. Express **24**(18), 20132–20142 (2016). https://doi.org/10.1364/OE.24.020132

S. Unterkofler, R.J. McQuitty, T.G. Euser, N.J. Farrer, P.J. Sadler, P.S.J. Russell, Microfluidic integration of photonic crystal fibers for online photochemical reaction analysis. Opt. Lett. **37**(11), 1952–1954 (2012). https://doi.org/10.1364/OL.37.001952

A.M. Vengsarkar, P.J. Lemaire, J.B. Judkins, V. Bhatia, T. Erdogan, J.E. Sipe, Long-period fiber gratings as band-rejection filters. J. Lightwave Technol. **14**(1), 58–64 (1996). https://doi.org/10.1109/50.476137

Y.P. Wang, D.N. Wang, W. Jin, Y.J. Rao, G.D. Peng, Asymmetric long period fiber gratings fabricated by use of CO_2 laser to carve periodic grooves on the optical fiber. Appl. Phys. Lett. **89**(15), 19–21 (2006). https://doi.org/10.1063/1.2360253

L. Wang, D. He, S. Feng, C. Yu, L. Hu, J. Qiu, D. Chen, Phosphate ytterbium-doped single-mode all-solid photonic crystal fiber with output power of 13.8 W. Sci. Rep. **5**, 10–13 (2015). https://doi.org/10.1038/srep08490

C. Wu, M.-L.V. Tse, Z. Liu, B.-O. Guan, C. Lu, H.-Y. Tam, In-line microfluidic refractometer based on C-shaped fiber assisted photonic crystal fiber Sagnac interferometer. Opt. Lett. **38**(17), 3283–3286 (2013). https://doi.org/10.1364/OL.38.003283

C. Wu, M.-L.V. Tse, Z. Liu, B.-O. Guan, A.P. Zhang, C. Lu, H.-Y. Tam, In-line microfluidic integration of photonic crystal fibres as a highly sensitive refractometer. The Analyst **139**(21), 5422–5429 (2014). https://doi.org/10.1039/C4AN01361A

N. Zhang, G. Humbert, Z. Wu, K. Li, P.P. Shum, N.M.Y. Zhang et al., In-line optofluidic refractive index sensing in a side-channel photonic crystal fiber. Opt. Express **24**(24), 419–424 (2016a). https://doi.org/10.1364/OE.24.027674

N. Zhang, G. Humbert, T. Gong, P.P. Shum, K. Li, J.-L. Auguste et al., Side-channel photonic crystal fiber for surface enhanced Raman scattering sensing. Sens. Actuators B Chem. **223**, 195–201 (2016b). https://doi.org/10.1016/j.snb.2015.09.087

N. Zhang, K. Li, Y. Cui, Z. Wu, P.P. Shum, J.-L. Auguste et al., Ultra-sensitive chemical and biological analysis via specialty fibers with built-in microstructured optofluidic channels. Lab Chip **18**(4), 655–661 (2018). https://doi.org/10.1039/C7LC01247K

T. Zhu, D. Wu, M. Liu, D.W. Duan, In-line fiber optic interferometric sensors in single-mode fibers. Sensors (Switzerland) **12**(8), 10430–10449 (2012). https://doi.org/10.3390/s120810430